





# Possible role for rare *TRPM7* variants in patients with hypomagnesaemia with secondary hypocalcaemia

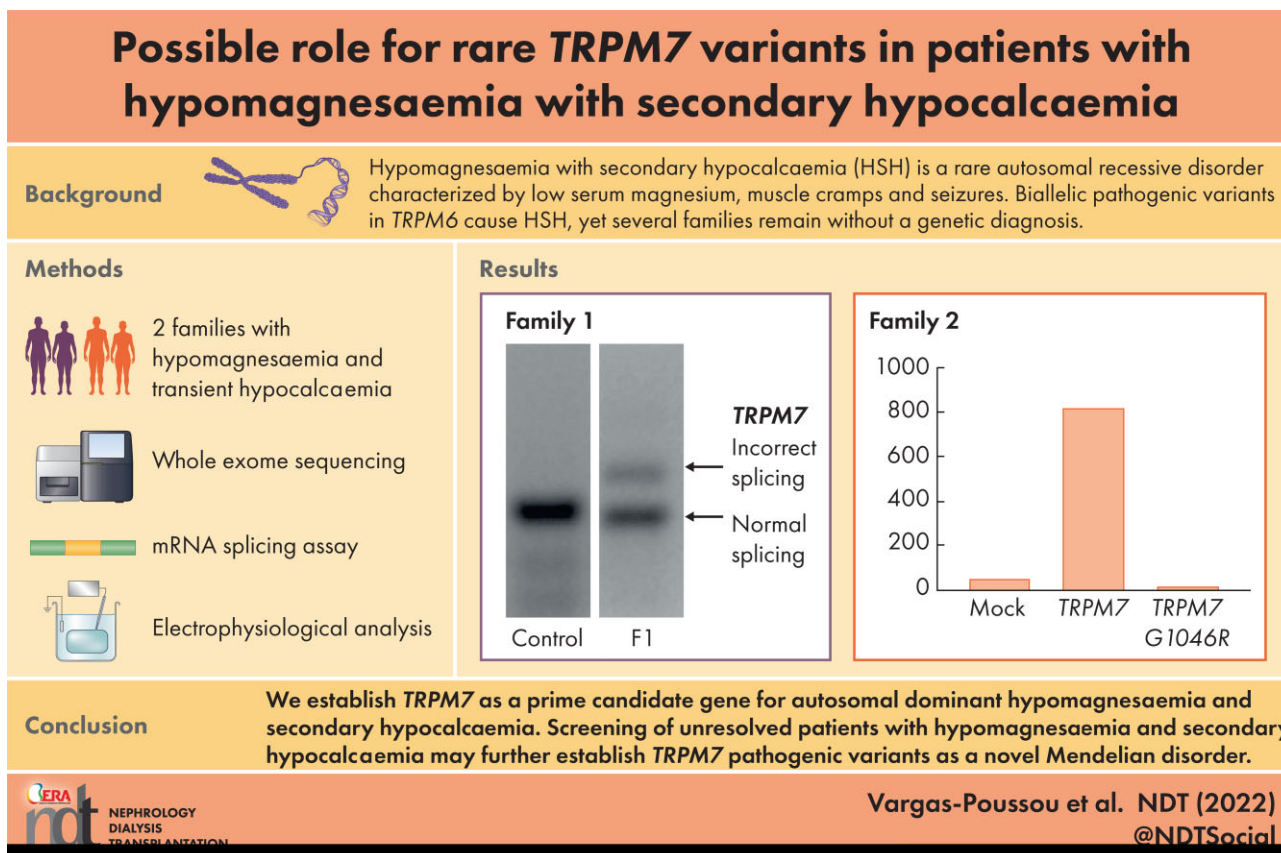
Rosa Vargas-Poussou <sup>1,\*</sup>, Felix Claverie-Martin<sup>2,\*</sup>, Caroline Prot-Bertoye<sup>3,4,5,\*</sup>, Valentina Carotti<sup>6</sup>, Jenny van der Wijst<sup>6</sup>, Ana Perdomo-Ramirez<sup>2</sup>, Gloria M. Fraga-Rodriguez<sup>7</sup>, Marguerite Hureauux<sup>1</sup>, Caro Bos <sup>6</sup>, Femke Latta<sup>6</sup>, Pascal Houillier<sup>3,4,5</sup>, Joost G.J. Hoenderop <sup>6</sup> and Jeroen H.F. de Baaij <sup>6</sup>

<sup>1</sup>Département de Génétique, Centre de référence des Maladies Rénales Héritaires de l'Enfant et de l'Adulte, Hôpital Européen Georges Pompidou, Paris, France, <sup>2</sup>Unidad de Investigación, Renal Tube Group, Hospital Universitario Nuestra Señora de Candelaria, Santa Cruz de Tenerife, Spain, <sup>3</sup>Centre de Recherche des Cordeliers, Sorbonne Université, INSERM, Université de Paris, CNRS, Paris, France, <sup>4</sup>Department of Physiology, Assistance Publique-Hôpitaux de Paris, Hôpital Européen Georges Pompidou, Paris, France, <sup>5</sup>Centre de Référence des Maladies Rénales Héritaires de l'Enfant et de l'Adulte, Paris, France, <sup>6</sup>Department of Physiology, Radboud Institute for Molecular Life Sciences, Radboud University Medical Center, Nijmegen, The Netherlands and <sup>7</sup>Sección de Nefrología Pediátrica, Hospital de la Santa Creu I Sant Pau, Barcelona, Spain

\*These authors contributed equally to this work.

Correspondence to: Jeroen H.F. de Baaij; E-mail: [jeroen.debaaij@radboudumc.nl](mailto:jeroen.debaaij@radboudumc.nl)

## GRAPHICAL ABSTRACT



## KEY LEARNING POINTS

### What is already known about this subject?

- Hypomagnesaemia with secondary hypocalcaemia (HSH) is a rare autosomal recessive disorder characterized by a very low serum magnesium concentration, muscle cramps and seizures.
- Biallelic pathogenic variants in *TRPM6* have been identified as the cause for HSH, yet several families remain without a genetic diagnosis.

### What this study adds?

- We report an autosomal dominant inheritance pattern of HSH.
- We describe for the first time the presence of rare variants in the *TRPM7* gene in patients with HSH.
- The identified variants result in defective splicing or impair *TRPM7* channel activity.

### What impact this may have on practice or policy?

- We recommend screening patients with HSH negative for variants in *TRPM6* for rare variants in *TRPM7*.
- Finding more *TRPM7* variants will improve diagnostics of patients with HSH, allowing genetic counseling.

## ABSTRACT

**Background.** Hypomagnesaemia with secondary hypocalcaemia (HSH) is a rare autosomal recessive disorder caused by pathogenic variants in *TRPM6*, encoding the channel-kinase transient receptor potential melastatin type 6. Patients have very low serum magnesium ( $Mg^{2+}$ ) levels and suffer from muscle cramps and seizures. Despite genetic testing, a subgroup of HSH patients remains without a diagnosis.

**Methods.** In this study, two families with an HSH phenotype but negative for *TRPM6* pathogenic variants were subjected to whole exome sequencing. Using a complementary combination of biochemical and functional analyses in overexpression systems and patient-derived fibroblasts, the effect of the *TRPM7*-identified variants on  $Mg^{2+}$  transport was examined.

**Results.** For the first time, variants in *TRPM7* were identified in two families as a potential cause for hereditary HSH. Patients suffer from seizures and muscle cramps due to magnesium deficiency and episodes of hypocalcaemia. In the first family, a splice site variant caused the incorporation of intron 1 sequences into the *TRPM7* messenger RNA and generated a premature stop codon. As a consequence, patient-derived fibroblasts exhibit decreased cell growth. In the second family, a heterozygous missense variant in the pore domain resulted in decreased *TRPM7* channel activity.

**Conclusions.** We establish *TRPM7* as a prime candidate gene for autosomal dominant hypomagnesaemia and secondary hypocalcaemia. Screening of unresolved patients with hypocalcaemia and secondary hypocalcaemia may further establish *TRPM7* pathogenic variants as a novel Mendelian disorder.

**Keywords:** genetics, HSH, magnesium deficiency, *TRPM6*, *TRPM7*

## INTRODUCTION

Hypomagnesaemia with secondary hypocalcaemia [HSH, (Mendelian Inheritance in Man #602014)] is a rare autosomal recessive disorder characterized by a very low serum magnesium ( $Mg^{2+}$ ) concentration ( $<0.3$  mmol/L) [1, 2].

Hypocalcaemia is a secondary effect of hypomagnesaemia as a consequence of parathyroid failure or parathyroid hormone (PTH) resistance [3]. Patients often present during the newborn period with severe seizures, which can result in severe neurological damage if left untreated.

In 2002, variants in *TRPM6* were identified to be causative for HSH [1, 2]. *TRPM6* encodes a non-selective divalent cation channel, transient receptor potential melastatin type 6 (*TRPM6*), with high permeability for  $Mg^{2+}$  [4, 5]. A recent study shows that *TRPM6* functions in tetramers with its close homologue *TRPM7* and that this interaction is essential for *TRPM6* activity [6]. Both channels are sensitive to intracellular  $Mg^{2+}$  and  $Mg$ -ATP levels and have differential concentration-dependent channel inhibition [7]. The activity of *TRPM6/TRPM7* tetramers is, therefore, regulated by the relative expression of *TRPM6* and *TRPM7* subunits. *TRPM6* decreases the  $Mg$ -adenosine triphosphate (ATP)-induced inhibition of *TRPM7* and thereby increases  $Mg^{2+}$  transport activity [6].

Whereas *TRPM7* is ubiquitously expressed throughout the body, *TRPM6* is exclusively located in epithelia, with the highest expression in the colon and kidney [8]. Within the kidney, *TRPM6/TRPM7* tetramers locate in the distal convoluted tubule (DCT) segment of the nephron, where they are believed to function as tetramers on the apical membrane [8–10]. Urinary  $Mg^{2+}$  excretion is ultimately determined in the DCT since no  $Mg^{2+}$  reabsorption takes place beyond this segment [11, 12]. As a consequence, impaired  $Mg^{2+}$  transport via *TRPM6/TRPM7* in the DCT inevitably results in renal  $Mg^{2+}$  wasting and hypomagnesaemia [1–3, 13].

The pathophysiology of HSH comprises a primary defect in intestinal  $Mg^{2+}$  uptake and additional renal  $Mg^{2+}$  wasting. During phases of severe hypomagnesaemia, the renal wasting is not detectable. It can, however, be evidenced after normalization of plasmatic levels ( $Mg^{2+}$  loading test). Here we report HSH in two families: one with an autosomal inheritance pattern and one *de novo*. Using whole exome sequencing (WES), we identified rare variants in *TRPM7* that were functionally evaluated using patch clamp electrophysiology and biochemical analyses.

## MATERIALS AND METHODS

### Patient analysis

Electrolytes in the blood and 24-h urine measurements of the patients were performed according to standard procedures. An intravenous  $Mg^{2+}$ -loading test was executed in individuals F1-II.2, F1-II.3 and F1-III.3. The probands of both families were subjected to WES, which, in the case of F1-II.2, was performed at BGI-Europe (Copenhagen, Denmark), employing a HiSeq 2000 machine (Illumina, San Diego, CA, USA). In the case of family 2, DNA samples were sent to Macrogen (Seoul, South Korea) and WES analysis was carried out using an Illumina platform. Candidate genes were selected and analysed in the other family members by Sanger sequencing. Full methods are available as Supplementary material.

### Messenger RNA (mRNA) analysis

Primary fibroblast cultures were established from a skin biopsy. mRNA isolation of patients' blood was performed using the PAXgene Blood RNA kit (Qiagen, Manchester, UK). Regions of interest were amplified using reverse transcription-polymerase chain reaction (PCR) and directly Sanger sequenced according to standard methods. To identify the sequences of the alternatively spliced *TRPM7*, a 5' rapid amplification of complementary DNA ends PCR was performed according to the manufacturer's protocol (Invitrogen, Carlsbad, CA, USA). Full methods are available as Supplementary material.

### Functional experiments

HEK293 cells were transfected with wild-type and mutant *TRPM7* constructs for 48 h. At the start of the  $^{25}Mg^{2+}$  uptake experiments, cells were transferred to  $Mg^{2+}$ -free medium supplemented with 1 mmol/L  $^{25}Mg^{2+}$  (purity  $\pm$  98%; Cortecnet, Voisins le Bretonneux, France). After 15 min, the buffer was removed and the cells were washed and lysed. Lysates were subjected to inductively coupled plasma mass spectrometry analysis. Full methods are available as Supplementary material.

## RESULTS

### Hypomagnesaemia with secondary hypocalcaemia

Two families were submitted for genetic testing under the suspicion of HSH (Fig. 1A). The first family, of French origin, presented with hypomagnesaemia (range 0.25–0.51 mmol/L) and episodes of hypocalcaemia in two affected family members (Fig. 1A, F1). All other serum electrolytes were in the normal range (Table 1). The proband (patient II.2, Fig. 1B) is a 78-year-old female with hypercholesterolaemia, hypertension and Hashimoto thyroiditis. Hypomagnesaemia and hypocalcaemia were discovered at the age of 68, when she was admitted for acute abdominal pain (plasma  $Mg^{2+}$  0.37 mmol/L); fasting urinary  $Mg^{2+}$  excretion was low as well (2.8  $\mu$ mol/L glomerular filtrate). Hypocalcaemia was

corrected by oral calcium carbonate (1500 mg/d), but oral  $Mg^{2+}$  failed to correct hypomagnesaemia. On anamnesis, the patient disclosed she had episodes of muscle cramps throughout her life. The brother of the proband (patient II.3) had a medical history of arterial hypertension, dyslipidaemia, chronic kidney disease (CKD) stage 4 and Grave's disease that required a full thyroidectomy. He had an episode of tetany at the age of 63, after thyroidectomy, initially ascribed to post-surgery hypoparathyroidism. Then hypocalcaemia [serum ionized calcium ( $Ca^{2+}$ ) 1.10 mmol/L] and an inappropriately low PTH concentration (14 pg/mL) were confirmed (Fig. 1C, May 2014); hypomagnesaemia (0.25 mmol/L) was present with low urinary  $Mg^{2+}$  excretion (0.29 mmol/day). Of note,  $Mg^{2+}$  infusion (see below) normalized both PTH and blood  $Ca^{2+}$  concentrations, showing that hypoparathyroidism was not a result of thyroid surgery but a consequence of hypomagnesaemia. An episode of generalized seizures occurred when he was 77; no other cause than hypomagnesaemia could be retrieved. The son of the proband (patient III.3, Fig. 1D) had hypomagnesaemia (0.53 mmol/L) diagnosed at the age of 47, during family screening. His medical history showed asthma and occasional episodes of paresthesia. The affected individuals presented with low urinary  $Mg^{2+}$  excretion at the basal state (0.72, 0.29, 0.29 mmol/day in patients II.2, II.3 and III.3, respectively). Patients III.1, III.2, IV.1 and IV.2 had normal plasma  $Mg^{2+}$  concentrations (Table 1). A  $Mg^{2+}$  loading test in patients II.2, II.3 and III.3 demonstrated both intestinal and renal  $Mg^{2+}$  (re)absorption defects in all patients, similar to what is observed in patients with loss-of-function of *TRPM6* [2] (Fig. 1E).

An unrelated child of Spanish origin was hospitalized with convulsions at the age of 7 months (Fig. 1A, F2). Nystagmus had been observed since birth. Blood analysis demonstrated the presence of severe hypomagnesaemia (0.44 mmol/L) (Table 1). Serum ionized  $Ca^{2+}$  levels were low during episodes of convulsions (0.94 mmol/L), but were restored to normal values.  $Mg^{2+}$  supplementation was unable to restore  $Mg^{2+}$  levels (0.51 mmol/L) and urinary  $Mg^{2+}$  excretion was increased (fractional excretion of magnesium 22%, normal value <2.2%) and was associated with low urinary calcium excretion. He did not present proteinuria (protein:creatinine ratio <22 mg/mmol) and PTH levels were in the normal range. Ultrasound evaluation showed normal kidneys. Since the first diagnosis, the patient has suffered repeatedly from seizures (epilepsy associated with psychomotor retardation). Other complementary examinations aimed at studying psychomotor retardation and epilepsy were negative. Both parents were healthy and had normal serum  $Mg^{2+}$  and  $Ca^{2+}$  levels (mother:  $Mg^{2+}$  0.77 mmol/L, total Ca 2.32 mmol/L; father:  $Mg^{2+}$  0.82 mmol/L,  $Ca^{2+}$  2.35 mmol/L).

### Identification of *TRPM7* variants

WES identified rare *TRPM7* variants in both families. A heterozygous chr15:50978727G>C (c.3+1 G>C) variant was found in family 1, which is located at the first position of intron 1 of the *TRPM7* gene. This substitution in the canonical

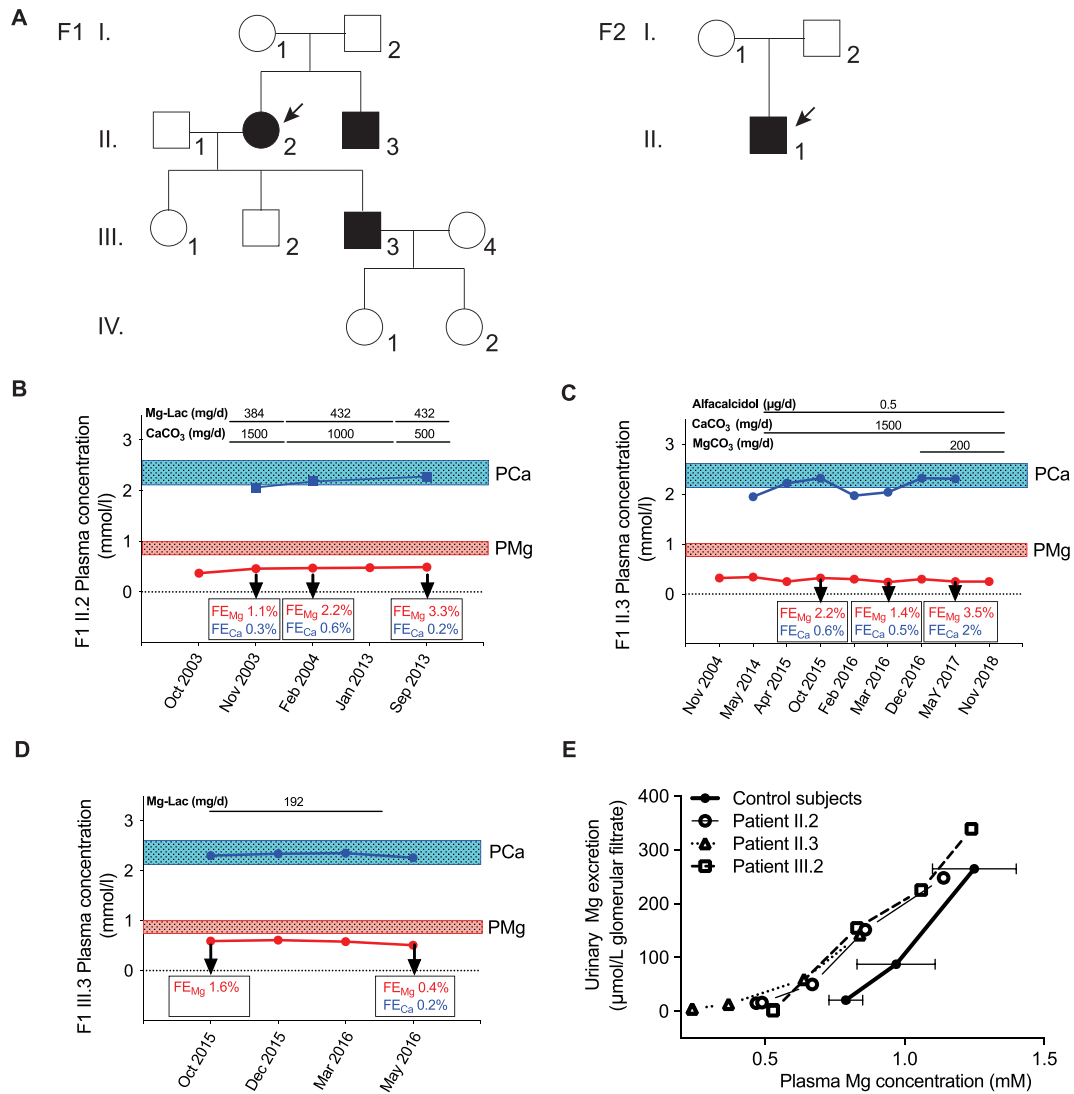


**FIGURE 1:** HSH phenotype in two families with a dominant inheritance pattern. (A) Pedigree of the families with autosomal dominant hypomagnesaemia and secondary hypocalcaemia. Black symbols denote affected and genetically confirmed family members. (B–D) Clinical course of patients F1-II.2, II.3 and III.3. (E) Mg<sup>2+</sup> loading test showing combined intestinal and renal Mg<sup>2+</sup> wasting in individuals F1-II.2, F1-II.3 and F1-III.3. In patients on baseline (fasting) conditions, plasma Mg concentration was low and urinary Mg excretion was low as well ( $7.4 \pm 6.6 \mu\text{mol/L}$  of glomerular filtrate), as expected under fasting conditions and in the same range as in control subjects under control conditions ( $19.2 \pm 1.9 \mu\text{mol/L}$  of glomerular filtrate), showing that no urinary loss of Mg is seen when plasma Mg concentration is low. Then plasma Mg increased during Mg infusion in patients and controls and urinary Mg increased as well. However, for any plasma Mg concentration, urinary Mg excretion was higher in patients than in controls, showing that renal tubular reabsorption is impaired in patients; this can be clearly seen for any plasma Mg concentration  $\geq 0.8 \text{ mmol/L}$ . Therefore we conclude that the defect in renal tubular Mg reabsorption in patients manifests when plasma Mg reabsorption is normal or high.

splice donor site is predicted to abolish the splicing score (Alamut splicing prediction module) (Fig. 2A–C). Subsequent Sanger sequencing of the patients and two non-affected family members indicated that the variant cosegregated with the hypomagnesaemia phenotype (Fig. 2A, Supplementary data, Figure S1). In family 2, a heterozygous chr15:50891345C>T (c.3137G>A) variant was identified in exon 22, resulting in a p.Gly1046Asp change (Fig. 2B). The Combined Annotation-Dependent Depletion (CADD)-Phred scaled CADD score for this variant was 27.8, which ranked it in the top of damaging variants, and was predicted pathogenic with very high scores

by the variant pathogenicity prediction tools PolyPhen-2 HVAR and SIFT. Parental testing by Sanger sequencing did not show the variant, indicating a *de novo* origin. Both identified variants were absent in our in-house database, dbSNP, the 1000-Genomes Project and the Genome Aggregation Database (gnomAD). Moreover, there were no rare variants detected in known hypomagnesaemia-causing genes [14–21]. Nor did we detect other rare variants that could explain the phenotype (Supplementary data, Tables S1–S4). The new *TRPM7* variants were submitted to ClinVar and were included with accession numbers VCV000974783 and SCV001482422.

**Table 1. Clinical data for families 1 and 2**

	Family 1			Family 2		
	Patient II-2	Patient II-3	Patient III-3	Unaffected subjects (n = 4)	Patient II-1	Normal values
Age (years)	78	76	48		3	
Height (cm)	155	167	170		98	
Weight (kg)	85.6	80.2	69.3		15.5	
Na <sup>+</sup> (mmol/L)	140	138	141		139	137–145
K <sup>+</sup> (mmol/L)	4.4	4.1	3.7		3.9	3.5–4.5
Cl <sup>-</sup> (mmol/L)	105	101	104		102	99–106
Total CO <sub>2</sub> (mmol/L)	22	24	25		29	23–28
Ca <sup>2+</sup> (mmol/L)	2.28	2.31	2.26	2.35 ± 0.04	2.59	2.1–2.6
Mg <sup>2+</sup> (mmol/L)	0.49	0.25	0.51	0.82 ± 0.04	0.61	0.7–1.0
Pi (mmol/L)	0.80	1.05	0.70		1.30	0.82–1.39
Creatinine (μmol/L)	101	226	75		44	<sup>a</sup> 53–97.2, <sup>b</sup> 61.9–114.9 and <sup>c</sup> 46–61
eGFR (mL/min/1.73 m <sup>2</sup> )	46	26	96		130	>90
Renin (pg/mL)	16.5	4.8	12.7		–	9–30
PTH (pg/mL)	72*	17*	49*		58.3**	*11–57, **14.5–87.1
Aldosterone (pmol/L)	168	270	216		–	80–1000
24-hr urine volume (mL)	1100	1185	1811		–	
Na <sup>+</sup> (mmol/day)	83	125	60			
FENa (%)					0.13	
K <sup>+</sup> (mmol/day)	39	39	54			
FEK (%)					5.78	
Cl <sup>-</sup> (mmol/day)	90	120	69			
FECl (%)					0.16	
Ca <sup>2+</sup> (mmol/day)	0.34	0.56	0.62			
Ca:Cr					0.02	
Mg <sup>2+</sup> (mmol/day)	0.89	0.19	0.29			
FEMg (%)					7.5	
Pi (mmol/day)	10.8	13.5	16.7			
TRP					84.58	

Estimated glomerular filtration rate (eGFR) was calculated by the Modification of Diet in Renal Disease formula (family 1) and by the Schwartz 2009 formula (family 2). FENa: fractional excretion of sodium; FEK: fractional excretion of potassium; FECl: fractional excretion of chloride; FEMg: fractional excretion of magnesium; Ca:Cr: calcium:creatinine ratio; TRP: tubular reabsorption of phosphate. Conversion factors: Ca<sup>2+</sup> mmol/L = mg/dL × 0.25; Mg<sup>2+</sup> mmol/L = mg/dL × 0.48; Pi mmol/L = mg/dL × 0.32; creatinine μmol/L = mg/dL × 88.5; renin mU/L = pg/mL × 1.65; aldosterone pmol/L = ng/dL × 27.75.

Reference values for the fractional excretions are not usually included since they depend on the levels of electrolytes in the serum and the volaemia. They are interpreted in a clinical context.

The asterisks indicate the reference values in the respective hospitals/countries.

<sup>a, b and c</sup> Creatinine normal values for adult women, men and children, respectively.

### TRPM7 splice donor variant results in alternative splicing and decreased cell growth

To examine the effects of the intronic *TRPM7* variant on splicing of the *TRPM7* mRNA, mRNA was isolated from the whole blood of patients II.2 and III.3. The PCR amplification of the spliced mRNA using primers in exon 1 and 2 demonstrated the presence of the normal spliced mRNA and also a larger band in minor quantities (Fig. 3A and B). Sanger sequencing of this band indicated that this transcript consists of several defective spliced mRNAs that all contain parts of intron 1. The most common transcript (~80% of all defective transcripts) includes the first part of intron 1 and splices from position +71 to exon 2 (Supplementary data, Figure S2). The defective splicing caused a frame shift and a premature stop codon close to the beginning of exon 2.

To determine the functional consequences of the defective splicing, fibroblasts were isolated from patient II.3. Fibroblasts express TRPM7 and are dependent on its function for cell growth and survival [22, 23]. Indeed, fibroblasts from patient II.3 show the presence of the incorrectly spliced mRNA transcript (Fig. 3C), but low-normal TRPM7 protein expression

(Fig. 3D). Proliferation assays showed that patient-derived fibroblasts demonstrated decreased cell growth (Fig. 3E). The decreased cell growth could not be rescued by culturing the cells in medium supplemented with 10 mM MgCl<sub>2</sub> or 50 μM zinc chloride (Fig. 3F).

### TRPM7 missense variant decreases the activity of the channel

The Gly1046 residue is located in the TRPM7 channel pore (Fig. 4A). The change of a hydrophobic glycine for the large side chain of aspartic acid and its negative charge is predicted to disturb the pore structure and interfere with the channel function. To determine the functional implications of the variant on TRPM7 channel activity, we performed electrophysiological recordings. Whole-cell patch clamp of mock-transfected cells displayed small endogenous outward currents (46 ± 11 pA/pF), while the averaged current density for wild-type TRPM7 was 838 ± 112 pA/pF (Fig. 4B and C). A significant decrease in current amplitude was observed for the p.Gly1046Asp mutant, which showed outward currents

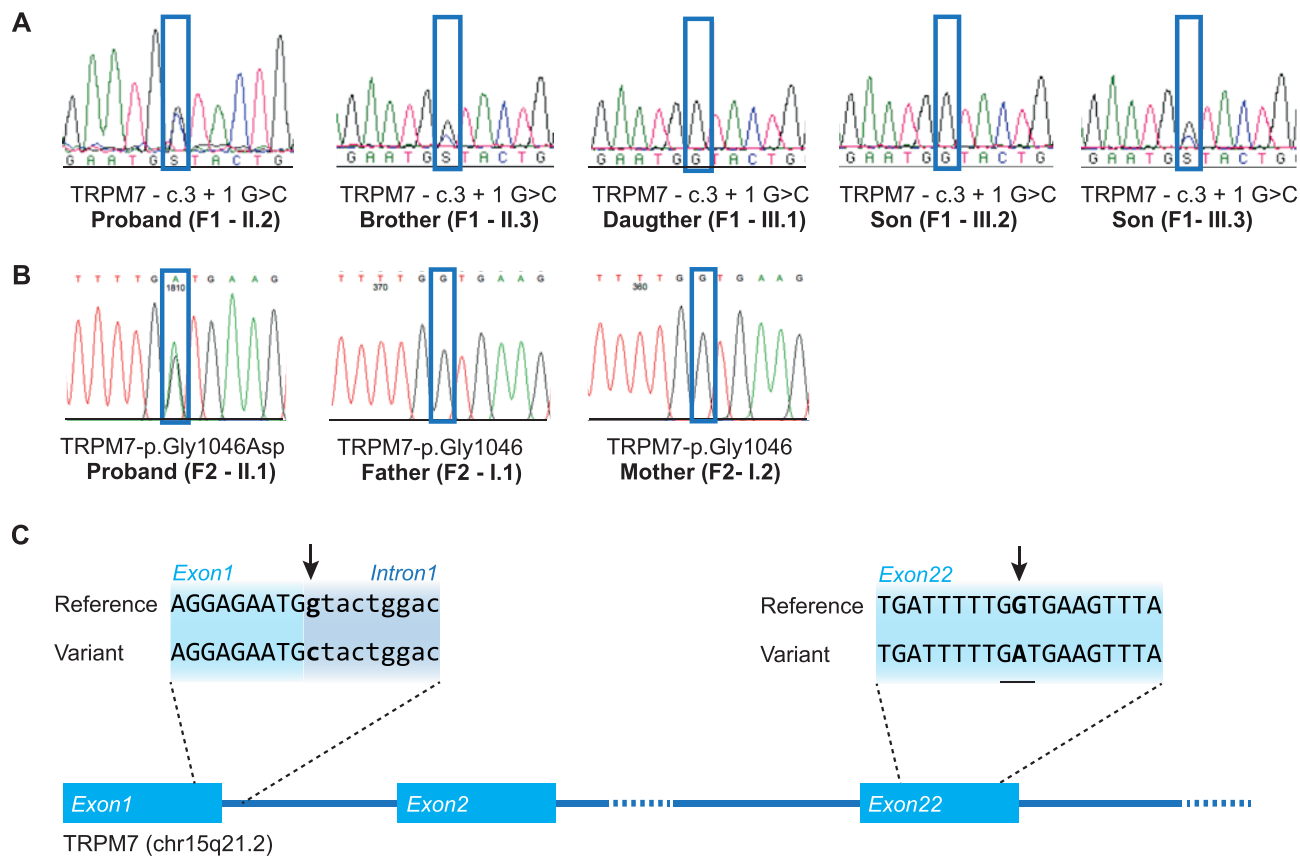


**FIGURE 2:** Identification of *TRPM7* mutations. (A) Mutation analysis chromatograms of F1, demonstrating the presence of the mutation in the proband (II.2), the brother of the proband (II.3) and one child of the proband (III.3). (B) Mutation analysis chromatograms of F2, demonstrating the presence of the mutation in the proband (II.1). (C) Affected family members from F1 carry a *TRPM7* splice site mutation at the first nucleotide of the first intron (c.3+1 G>C). The *de novo* mutation in F2 is located in exon 22 and results in a p.Gly1046Asp missense mutation. Mutations are indicated by the black arrows.

comparable to the mock-transfected cells ( $22 \pm 4$  pA/pF;  $P > .99$ ).  $^{25}\text{Mg}^{2+}$  uptake experiments demonstrated that HEK293 cells overexpressing TRPM7-p.Gly1046Asp show comparable uptake to mock-transfected cells (Fig. 4D). The TRPM7-mediated  $^{25}\text{Mg}^{2+}$  uptake was significantly inhibited by the specific TRPM7 inhibitor NS8593 (Fig. 4E) [24]. Interestingly,  $^{25}\text{Mg}^{2+}$  uptake in both mock- and TRPM7-p.Gly1046Asp-expressing cells was decreased by NS8593, suggesting that the mutant has no dominant negative effect on endogenous TRPM7 activity (Fig. 4E). Cell-surface biotinylation showed that wild-type TRPM7 and TRPM7-p.Gly1046Asp are both expressed at the plasma membrane (Fig. 4F and G). Of note, the expression of TRPM7-p.Gly1046Asp in cell lysate and plasma membrane fractions was marginally lower than wild-type TRPM7.

In the kidney, TRPM7 functions in homotetrameric complexes or in heterotetrameric complexes with TRPM6 to facilitate  $\text{Mg}^{2+}$  reabsorption. To further examine whether TRPM7-p.Gly1046Asp has a dominant negative effect on wild-type TRPM7 activity, TRPM7 wild-type and TRPM7-p.Gly1046Asp plasmids were cotransfected in HEK293 cells. Cells co-expressing TRPM7 and TRPM7-p.Gly1046Asp showed a comparable current density to TRPM7- and mock-expressing cells ( $260 \pm 70$  versus  $497 \pm 84$  pA/pF;  $P = .34$ ; Fig. 5A and B). Of note, cells cotransfected with TRPM7 and mock

plasmids showed a decreased current density compared with TRPM7-expressing cells, in line with 50% lower expression levels (Fig. 5B). Indeed, co-expression of wild-type TRPM7 and TRPM7-p.Gly1046Asp resulted in similar  $^{25}\text{Mg}^{2+}$  uptake as cells transfected with TRPM7 and mock ( $P = .79$ ; Fig. 5C), demonstrating that wild-type TRPM7 activity is not decreased by the presence of the mutant. Similar results were obtained when co-expressing TRPM6 and TRPM7. In line with previous studies [6], co-expression of TRPM7 significantly increases the TRPM6 current density ( $742 \pm 116$  pA/pF) (Fig. 5D and E). In contrast, cells expressing TRPM7-p.Gly1046Asp and TRPM6 displayed a current density similar to cells with TRPM6 and mock ( $240 \pm 56$  versus  $320 \pm 61$  pA/pF;  $P = .93$ ), indicating that TRPM7-p.Gly1046Asp did not affect TRPM6 current density (Fig. 5D and E). Cell surface biotinylation of TRPM7 and TRPM7-p.Gly1046Asp demonstrated equal TRPM7 expression among all conditions (Fig. 5F and G).

## DISCUSSION

Here we report two families with hypomagnesaemia and secondary hypocalcaemia. WES identified a pathogenic *de novo* missense variant that alters the *TRPM7* channel pore and a splice site variant that results in defective splicing of *TRPM7* transcripts. Our results establish the *TRPM7* gene as a prime

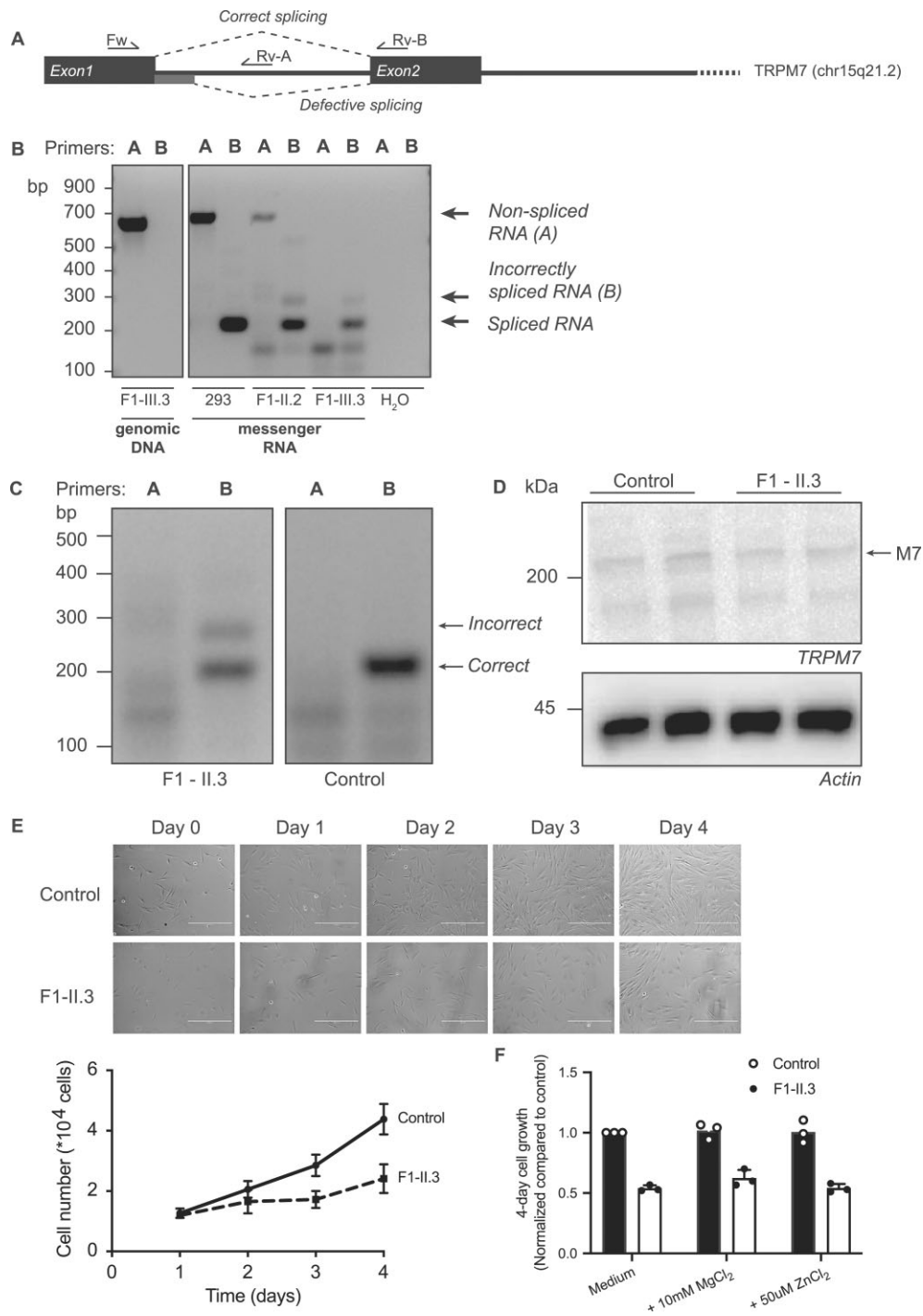


**FIGURE 3:** mRNA analysis demonstrates defective splicing of *TRPM7* in family 1. (A) Schematic overview of the *TRPM7* gene, indicating the primer locations and the correct and defective splice sites. (B) mRNA analysis of the non-spliced (primer set A) and spliced (primer set B) first intron of *TRPM7* using mRNA isolated from blood of the proband (F1-II.2) and individual F1-III.3. As controls, water, genomic DNA and mRNA from HEK293 cells were included. The analysis shows the presence of alternatively spliced mRNA in the patient samples, indicated with an arrow. (C) mRNA splicing analysis using mRNA from fibroblasts shows the presence of alternatively spliced mRNA in individual F1-II.3, indicated with an arrow. (D) Representative immunoblot demonstrating the protein expression of TRPM7 in control fibroblasts and fibroblasts from individual F1-II.3. Actin was used as a loading control. (E) Cell proliferation was determined by cell counting during 4 days of culture and shows decreased cell growth in fibroblasts from individual F1-II.3. Representative images of control and F1-II.3 fibroblasts are shown in the top panel. (F) Cell proliferation could not be rescued by the addition of MgCl<sub>2</sub> or ZnCl<sub>2</sub>. Graphs show the mean of three independent experiments, which each contained three replicates  $\pm$  standard error of the mean.

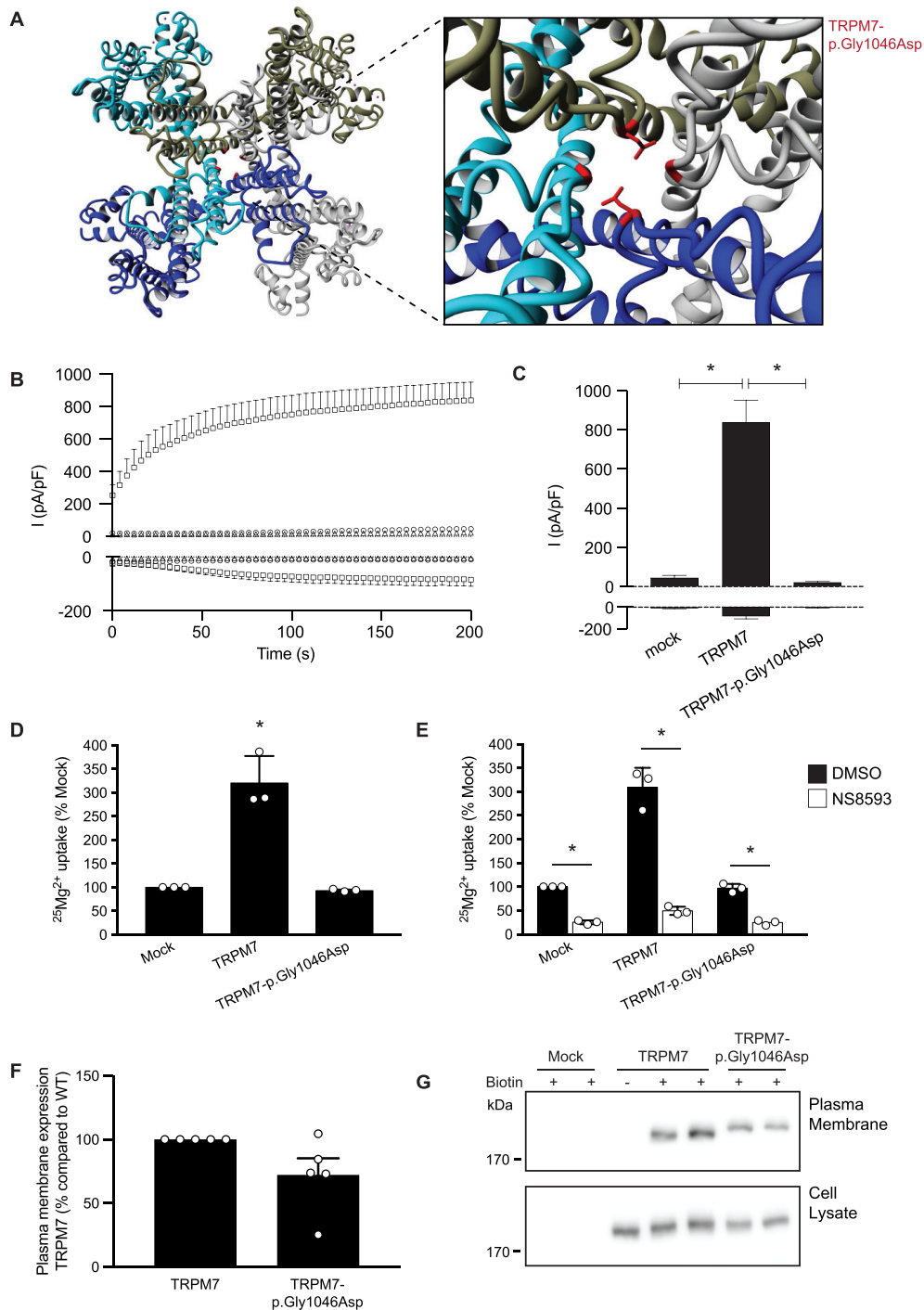


**FIGURE 4:** The TRPM7-p.Gly1046Asp mutant of family 2 results in decreased  $Mg^{2+}$  uptake. **(A)** Molecular modelling using the structure of human TRPM7 (pdb: 5ZX5). The outtake shows the heterozygous p.Gly1046Asp mutation present in two out of the four subunits of the channel. **(B)** Averaged time course of outward (+80 mV) and inward (-80 mV) from HEK293 cells transfected with *TRPM7* wild-type (squares,  $n = 9$ ) or *TRPM7-p.Gly1046Asp* (triangles,  $n = 9$ ) and non-transfected HEK293 cells as control (circles,  $n = 6$ ). **(C)** Bar graph presenting the current densities at +80 mV and -80 mV of indicated conditions at 200 s after establishing whole-cell configuration. Mean + standard error of the mean (SEM) is shown. An asterisk indicates significance compared with TRPM7 wild-type. **(D and E)**  $^{25}Mg^{2+}$  uptake assay of HEK293 cells expressing mock, wild-type *TRPM7* and mutant *TRPM7-p.Gly1046Asp*. Cells were incubated for 15 min in a buffer containing 1 mM  $^{25}Mg^{2+}$  (98% purity) in the presence or absence of 0.4 (v/v)% DMSO (E, black bars) or 30  $\mu M$  NS8593 (E, white bars). Intracellular  $^{25}Mg^{2+}$  content was measured by inductive-coupled plasma mass spectrometry. Graphs show the mean of three independent experiments, which each contained three replicates  $\pm$  standard deviation; \* $P < .05$  compared with mock (D) or DMSO (E). **(F and G)** Immunoblots showing similar membrane expression between TRPM7 proteins (upper blot) and a TRPM7 expression control (lower blot). The quantifications show the mean  $\pm$  SEM of five independent experiments.



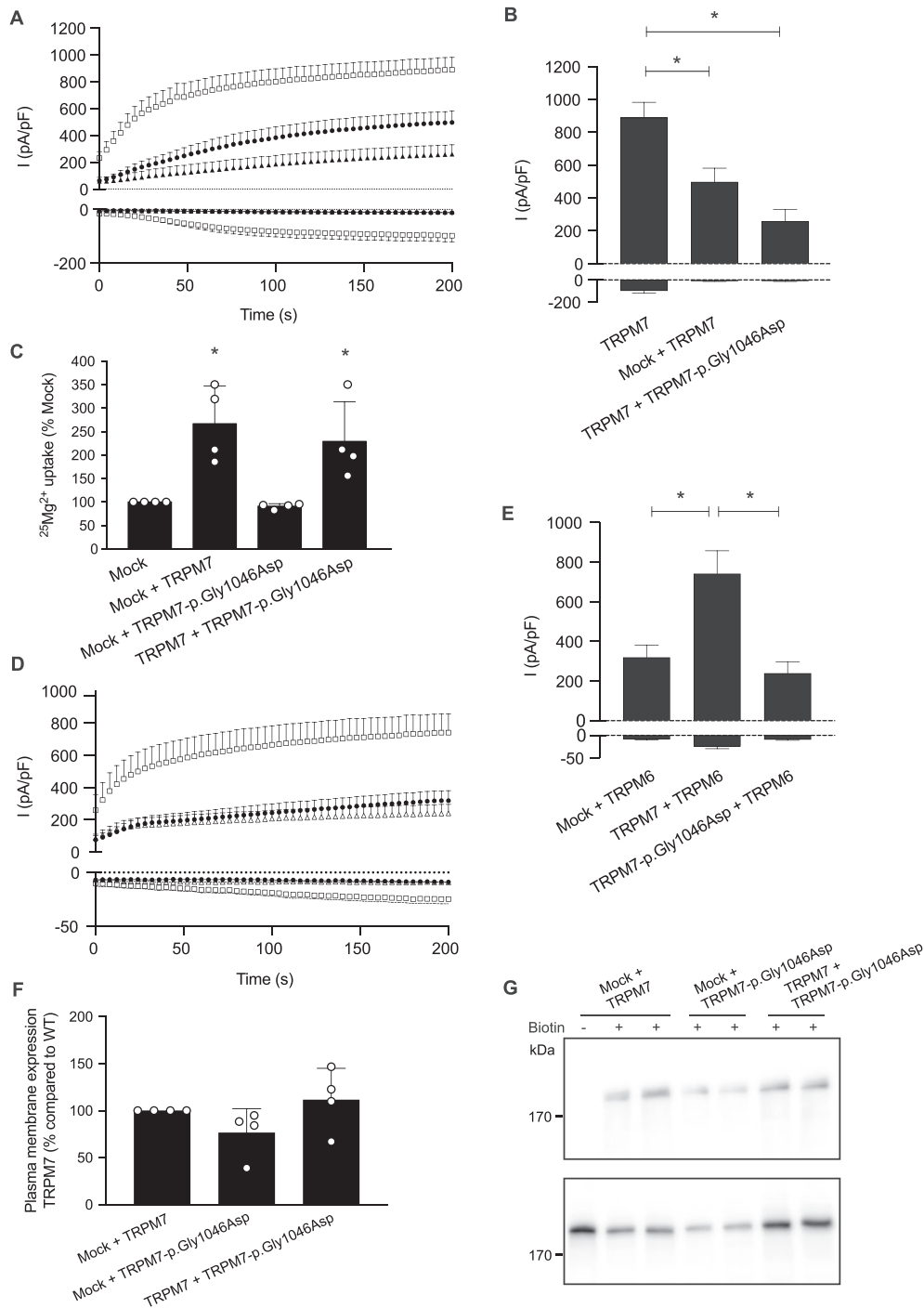


**FIGURE 5:** The TRPM7-p.Gly1046Asp mutant does not affect the wild-type TRPM7 activity. **(A and B)** Whole-cell patch clamp recordings with **(A)** averaged time course of outward (+80 mV) and inward (−80 mV) current densities from HEK293 cells transfected with either *TRPM7* wild-type (open squares,  $n = 17$ ) alone or cotransfected with either *TRPM7* wild-type and mock (closed circles,  $n = 7$ ) or *TRPM7* wild-type and *TRPM7*-p.Gly1046Asp (closed triangles,  $n = 9$ ). Bar graph **(B)** presenting the current densities at +80 mV and −80 mV of indicated conditions at 200 s after establishing whole-cell configuration. Mean + standard error of the mean (SEM) is shown. An asterisk indicates significance ( $P < .05$ ). **(C)**  $^{25}\text{Mg}^{2+}$  uptake assay of HEK293 cells co-expressing mock, wild-type TRPM7 and mutant TRPM7-p.Gly1046Asp. Cells were incubated for 15 min in a buffer containing 1 mM  $^{25}\text{Mg}^{2+}$  (98% purity). Intracellular  $^{25}\text{Mg}^{2+}$  content was measured by inductive-coupled plasma mass spectrometry. Graphs show the mean of three independent experiments, which each contained three replicates  $\pm$  standard deviation;  $*P < .05$  compared with mock. **(D and E)** Whole-cell patch clamp recordings with **(D)** averaged time course of outward (+80 mV) and inward (−80 mV) current densities from HEK293 cells cotransfected with TRPM6 wild-type and TRPM7 wild-type (open squares,  $n = 13$ ), TRPM6 wild-type and mock (closed circles,  $n = 15$ ) and TRPM6 wild-type and TRPM7-p.Gly1046Asp (open triangles,  $n = 12$ ). Bar graph **(E)** presenting the current densities at +80 mV and −80 mV of indicated conditions at 200 s after establishing whole-cell configuration. Mean + SEM is shown. An asterisk indicates significance ( $P < .05$ ). **(F and G)** Immunoblots showing comparable membrane expression between TRPM7 proteins (upper blot) and a TRPM7 expression control (lower blot). The semiquantifications show the mean  $\pm$  SEM of five independent experiments.

candidate for *de novo* and autosomal dominant inheritance of HSH.

Our results show for the first time the autosomal dominant inheritance of HSH. The cardinal symptom in our patients is hypomagnesaemia, which was associated with renal  $Mg^{2+}$  wasting. Additionally, intestinal  $Mg^{2+}$  malabsorption was demonstrated by an  $Mg^{2+}$  loading test in patients F1-II.2, II.3 and III.3. In line with HSH patients with *TRPM6* pathogenic variants, hypocalcaemia was not detected in all measurements but generally only during episodes of hypoparathyroidism. The presence of hypocalcaemia secondary to hypomagnesaemia is commonly explained by decreased PTH secretion [3]. Although the mechanism for decreased PTH secretion in chronic hypomagnesaemia is still not completely clear, it has been postulated that the inhibition of PTH secretion is caused by increased activity of the alpha subunit of the G protein downstream of the calcium-sensing receptor [25, 26]. Indeed, hypocalcaemia accompanied by a PTH level in the low-normal range was detected in patient F1-II.3. Hypocalcaemia was relieved by  $Mg^{2+}$  supplementation in all subjects.

The identification of two rare variants in *TRPM7* in two independent families suggests that *TRPM7* variants may be causative for autosomal dominant HSH. Nevertheless, it should be noted that the gnomAD lists a large number of observed missense variants in *TRPM7* compared with the missense expected: 756 versus 950 ( $Z$  score = 2.23). Although this suggests that *TRPM7* is relatively tolerant to missense variants, it should be noted that this score does not exclude pathogenicity of individual variants. Importantly, gnomAD does not list any nonsense or missense variants in residues that form the cation-specific pore domain: E1047, G1046 and F1045. In line with this observation, missense variants are also absent for the lower gate residue N1097 and the cysteine residues forming the pore disulfide bond: C1056 and C1066. Indeed, we demonstrate that the identified variants have functional consequences: the splice site variant impaired splicing of the first exon resulting in a premature stop codon and the p.Gly1046Asp variant was demonstrated to induce loss-of-function in patch clamp analysis. Moreover, *TRPM7* has a low loss-of-function observed/expected upper bound fraction (LOEUF) score of 0.56 in gnomAD [27], which is comparable to genes that are essential for human cell viability (mean LOEUF = 0.63). Although this may be indicative of pathogenicity, we feel that the identification of more families with *TRPM7* pathogenic variants is essential to provide a definitive answer.

To date, *TRPM6* has been considered as the main determinant of intestinal and renal  $Mg^{2+}$  (re)absorption [12, 28]. *TRPM6* channel activity is highly regulated by  $Mg^{2+}$ , ATP and hormonal factors [5, 29–31]. Pathogenic variants in *TRPM6* cause HSH and result in very low serum  $Mg^{2+}$  levels [1–3]. Our findings indicate that the presence of *TRPM7* may be equally important for renal and intestinal  $Mg^{2+}$  uptake. Indeed, both zebrafish and intestine-specific knockout mouse models of *TRPM7* demonstrate decreased serum  $Ca^{2+}$  and  $Mg^{2+}$  levels [9, 32].

Recently, using *TRPM7*-deficient trophoblast cells, Chubanov *et al.* [6] showed that *TRPM6* activity requires the presence of *TRPM7*. *TRPM6/TRPM6*

homotetramers are not functional, whereas *TRPM6/TRPM7* heterotetramers have increased  $Mg^{2+}$  transport activity compared with *TRPM7/TRPM7* homotetramers [6, 7]. *TRPM7/TRPM7* homotetramers are more susceptible to concentration-dependent inhibition by cytosolic Mg-ATP than *TRPM6/TRPM7* heterotetramers [6]. The heterozygous *TRPM7* variants cause decreased expression of *TRPM7*, which may result in more non-functional *TRPM6/TRPM6* homotetramers and fewer *TRPM6/TRPM7* heterotetramers. Thus the total  $Mg^{2+}$  (re)absorption capacity will be decreased, as shown by the  $Mg^{2+}$  loading test in all affected individuals of family 1.

In multiple cell systems and animal models, *TRPM7* has been shown to be essential for life [9, 22, 23, 33, 34]. *TRPM7* knockout impairs cell proliferation and therefore the channel is considered as the main determinant of intracellular  $Mg^{2+}$  levels [33]. Of note, the importance of *TRPM7* in  $Mg^{2+}$  homeostasis has also been questioned by some studies, since the deletion of *TRPM7* in T lymphocytes did not affect cellular  $Mg^{2+}$  handling [34]. However, *TRPM7*-deficient mice demonstrated that *TRPM7* is essential for the organismal balance of zinc ( $Zn^{2+}$ ),  $Mg^{2+}$  and  $Ca^{2+}$ . Indeed, the channel pore of *TRPM7* is permeable to  $Zn^{2+}$ ,  $Mg^{2+}$  and  $Ca^{2+}$  [9]. Interestingly, patient-derived fibroblasts show decreased growth rates. However, this growth could not be rescued by  $Mg^{2+}$  or  $Zn^{2+}$  supplementation.

Although *TRPM7* is considered necessary for cell survival, it is important to note that the reported variants are present in a heterozygous state and will not completely impair *TRPM7* function. The unique splice site variant reported here will not affect functional channels and will only result in haplotype insufficiency. Moreover, our  $^{25}Mg^{2+}$  uptake and patch clamp experiments demonstrated that the missense variant does not have a dominant negative effect on the functional wild-type protein. This may explain the relatively mild phenotype compared with knockout cells and mice [22, 23]. As heterozygous mice also have one functional allele, it is interesting to compare the patients with the *TRPM7*-deficient mice with the deletion of the alpha-kinase domain that were generated by Ryazanova *et al.* [23]. Heterozygous *TRPM7* $\Delta$ kinase mice were viable and had a defect in intestinal  $Mg^{2+}$  absorption, which is also present in family 1. Cells taken from heterozygous *TRPM7* $\Delta$ kinase mice demonstrated decreased *TRPM7* activity.

A limitation of our study is the identification of only two families with pathogenic variants in *TRPM7*. One may speculate that variants in *TRPM7* with more severe pathogenicity that entirely impair *TRPM7* function are not compatible with life. Indeed, rare variants in *TRPM7* have been associated with stillbirth [35]. Unfortunately, the  $Mg^{2+}$  status of the affected children is unknown. Our study suggests that the location of the variant may contribute to the severity of the disease. The fibroblasts from family 1 showed a significant *TRPM7* expression despite the heterozygous splice site variant, which may also be reflected in the older age of presentation of the patients. The strength of our study is the extensive phenotypic characterization of the patient's phenotype, including the  $Mg^{2+}$  loading test, clearly demonstrating a mixed phenotype of intestinal and renal mal(re)absorption.

In conclusion, we describe for the first time heterozygous pathogenic variants in *TRPM7* in patients with HSH. *TRPM7* should be screened in patients with an autosomal dominant inheritance pattern or individual cases with low blood  $Mg^{2+}$  levels.

## SUPPLEMENTARY DATA

Supplementary data are available at [ndt](#) online.

## ACKNOWLEDGEMENTS

We thank Willem Bosman and Gijs Franken for excellent technical support and Dr Hanka Venselaar for the visualization of the protein structure.

## FUNDING

This work was financially supported by ZonMW under the frame of the European Joint Programme on Rare Diseases (EJPRD2019-40) and by the IMAGEN project, which is cofunded by the PPP Allowance made available by Health~Holland, Top Sector Life Sciences & Health, to stimulate public-private partnerships (Implementation of Advancements in GENetic Kidney Disease, LSHM20009) and the Dutch Kidney Foundation (20OP+018). In addition, this project has received funding from the European Union's Horizon 2020 research and innovation programme under the EJP RD COFUND-EJP No 825575 and the Netherlands Organization for Scientific Research (NWO Veni 016.186.012. Vici 016.130.668). Work in Santa Cruz de Tenerife was financially supported by grant PI17/00153 (to F.C.M. and A.P.R.), integrated in the Plan Nacional de I+D+I 2013-2016 and co-financed by the ISCIII-Subdirección General de Evaluación y Fomento de la Investigación and the European Regional Development Fund 'Another way to build Europe'.

## AUTHORS' CONTRIBUTIONS

R.V.P., R.C.M., P.H., J.H., F.C.M. and J.d.B. designed the research studies. R.V.P., F.C.M., C.P.B., G.M.F.R. and P.H. acquired clinical data. V.C., J.v.d.W., C.B., F.L., J.d.B., A.P.R and F.C.M. conducted experiments and/or analysed data. R.V.P., F.C.M., P.H. and J.d.B. wrote the manuscript. All authors corrected the manuscript and approved the final version.

## CONFLICT OF INTEREST STATEMENT

None declared.

## REFERENCES

- Schlingmann KP, Weber S, Peters M *et al.* Hypomagnesaemia with secondary hypocalcemia is caused by mutations in *TRPM6*, a new member of the TRPM gene family. *Nat Genet* 2002; 31: 166–170
- Walder RY, Landau D, Meyer P *et al.* Mutation of *TRPM6* causes familial hypomagnesaemia with secondary hypocalcemia. *Nat Genet* 2002; 31: 171–174
- Schlingmann KP, Sassen MC, Weber S *et al.* Novel *TRPM6* mutations in 21 families with primary hypomagnesaemia and secondary hypocalcemia. *J Am Soc Nephrol* 2005; 16: 3061–3069
- Li M, Jiang J, Yue L. Functional characterization of homo- and heteromeric channel kinases *TRPM6* and *TRPM7*. *J Gen Physiol* 2006; 127: 525–537
- Li M, Du J, Jiang J *et al.* Molecular determinants of  $Mg^{2+}$  and  $Ca^{2+}$  permeability and pH sensitivity in *TRPM6* and *TRPM7*. *J Biol Chem* 2007; 282: 25817–25830
- Chubanov V, Ferioli S, Wisnowsky A *et al.* Epithelial magnesium transport by *TRPM6* is essential for prenatal development and adult survival. *eLife* 2016; 5: e20914
- Ferioli S, Zierler S, Zaisserer J *et al.* *TRPM6* and *TRPM7* differentially contribute to the relief of heteromeric *TRPM6/7* channels from inhibition by cytosolic  $Mg^{2+}$  and Mg-ATP. *Sci Rep* 2017; 7: 8806
- Voets T, Nilius B, Hoefs S *et al.* *TRPM6* forms the  $Mg^{2+}$  influx channel involved in intestinal and renal  $Mg^{2+}$  absorption. *J Biol Chem* 2004; 279: 19–25
- Mittermeier L, Demirkhanyan L, Stadlbauer B *et al.* *TRPM7* is the central gatekeeper of intestinal mineral absorption essential for postnatal survival. *Proc Natl Acad Sci USA* 2019; 116: 4706–4715
- Robak P, Ożgo M, Michałek K *et al.* Identification of *TRPM6* and *TRPM7* expression changes in response to a diet supplemented with inulin in porcine kidney. *Arch Anim Breed* 2016; 59: 267–274
- de Baaij JH, Hoenderop JG, Bindels RJ. Regulation of magnesium balance: lessons learned from human genetic disease. *Clin Kidney J* 2012; 5: i15–i24
- de Baaij JH, Hoenderop JG, Bindels RJ. Magnesium in man: implications for health and disease. *Physiol Rev* 2015; 95: 1–46
- Lainez S, Schlingmann KP, van der Wijst J *et al.* New *TRPM6* missense mutations linked to hypomagnesaemia with secondary hypocalcemia. *Eur J Hum Genet* 2014; 22: 497–504
- Arjona FJ, de Baaij JH, Schlingmann KP *et al.* *CNNM2* mutations cause impaired brain development and seizures in patients with hypomagnesaemia. *PLoS Genet* 2014; 10: e1004267
- Bockenbauer D, Feather S, Stanescu HC *et al.* Epilepsy, ataxia, sensorineural deafness, tubulopathy, and *KCNJ10* mutations. *N Engl J Med* 2009; 360: 1960–1970
- de Baaij JH, Dorresteijn EM, Hennekam EA *et al.* Recurrent *FXD2* p.Gly41Arg mutation in patients with isolated dominant hypomagnesaemia. *Nephrol Dial Transplant* 2015; 30: 952–957
- Ferre S, de Baaij JH, Ferreira P *et al.* Mutations in *PCBD1* cause hypomagnesaemia and renal magnesium wasting. *J Am Soc Nephrol* 2014; 25: 574–586
- Groenestege WM, Thebault S, van der Wijst J *et al.* Impaired basolateral sorting of pro-EGF causes isolated recessive renal hypomagnesaemia. *J Clin Invest* 2007; 117: 2260–2267
- Schlingmann KP, Bandulik S, Mammen C *et al.* Germline de novo mutations in *ATP1A1* cause renal hypomagnesaemia, refractory seizures, and intellectual disability. *Am J Hum Genet* 2018; 103: 808–816
- Schlingmann KP, Renigunta A, Hoorn EJ *et al.* Defects in *KCNJ16* cause a novel tubulopathy with hypokalemia, salt wasting, disturbed acid-base homeostasis, and sensorineural deafness. *J Am Soc Nephrol* 2021; 32: 1498–1512
- van der Wijst J, Konrad M, Verkaar SAJ *et al.* A de novo *KCNA1* mutation in a patient with tetany and hypomagnesaemia. *Nephron* 2018; 139: 359–366
- Nadler MJ, Hermosura MC, Inabe K *et al.* *LTRPC7* is a Mg-ATP-regulated divalent cation channel required for cell viability. *Nature* 2001; 411: 590–595
- Ryazanova LV, Rondon LJ, Zierler S *et al.* *TRPM7* is essential for  $Mg^{2+}$  homeostasis in mammals. *Nat Commun* 2010; 1: 109
- Chubanov V, Ferioli S, Gudermann T. Assessment of *TRPM7* functions by drug-like small molecules. *Cell Calcium* 2017; 67: 166–173
- Quitterer U, Hoffmann M, Freichel M *et al.* Paradoxical block of parathormone secretion is mediated by increased activity of G alpha subunits. *J Biol Chem* 2001; 276: 6763–6769
- Rodriguez-Ortiz ME, Canalejo A, Herencia C *et al.* Magnesium modulates parathyroid hormone secretion and upregulates parathyroid receptor expression at moderately low calcium concentration. *Nephrol Dial Transplant* 2014; 29: 282–289
- Karczewski KJ, Francioli LC, Tiao G *et al.* The mutational constraint spectrum quantified from variation in 141,456 humans. *Nature* 2020; 581: 434–443

28. Schaffers OJM, Hoenderop JGJ, Bindels RJM *et al.* The rise and fall of novel renal magnesium transporters. *Am J Physiol Renal Physiol* 2018; 314: F1027–F1033
29. Thebault S, Alexander RT, Tiel Groenestege WM *et al.* EGF increases TRPM6 activity and surface expression. *J Am Soc Nephrol* 2009; 20: 78–85
30. Nair AV, Hocher B, Verkaart S *et al.* Loss of insulin-induced activation of TRPM6 magnesium channels results in impaired glucose tolerance during pregnancy. *Proc Natl Acad Sci U S A* 2012; 109: 11324–11329
31. de Baaij JH, Blanchard MG, Lavrijsen M *et al.* P2X4 receptor regulation of transient receptor potential melastatin type 6 (TRPM6) Mg<sup>2+</sup> channels. *Pflugers Arch* 2014; 466: 1941–1952
32. Elizondo MR, Budi EH, Parichy DM. *trpm7* Regulation of *in vivo* cation homeostasis and kidney function involves stanniocalcin 1 and *fgf23*. *Endocrinology* 2010; 151: 5700–5709
33. Schmitz C, Perraud AL, Johnson CO *et al.* Regulation of vertebrate cellular Mg<sup>2+</sup> homeostasis by TRPM7. *Cell* 2003; 114: 191–200
34. Jin J, Desai BN, Navarro B *et al.* Deletion of *TRPM7* disrupts embryonic development and thymopoiesis without altering Mg<sup>2+</sup> homeostasis. *Science* 2008; 322: 756–760
35. Cartwright JH, Aziz Q, Harmer SC *et al.* Genetic variants in *TRPM7* associated with unexplained stillbirth modify ion channel function. *Hum Mol Genet* 2020; 29: 1797–1807

Received: 15.11.2021; Editorial decision: 22.4.2022